AIChE WILEY InterScience DISCOVER SOMETHING GREAT

An Integrated Methodology to Evaluate Permeability from Measured Microstructures

C. Selomulya
Dept. of Chemical Engineering, Faculty of Engineering, Clayton Campus, Monash University, Melbourne VIC 3800, Australia

T. M. Tran
ARC Centre for Functional Nanomaterials, School of Chemical Engineering and Industrial Chemistry, The University of New South Wales, Sydney NSW 2052, Australia

X. Jia and R. A. Williams
Institute of Particle Science and Engineering, School of Process, Environmental, and Materials Engineering, University of Leeds, Leeds LS2 9JT, United Kingdom

DOI 10.1002/aic.10967
Published online August 21, 2006 in Wiley InterScience (www.interscience.wiley.com).

Most existing data on solids dewatering behavior are based on macroscale phenomena and are often empirically based, whereas challenges still remain for fundamental understanding at a much smaller length scale. Prediction of microscale properties is now possible with enabling technologies such as X-ray microtomography (XMT) for 3-D imaging of solid structures and the Lattice–Boltzmann method (LBM) for calculating their permeability. Microstructural information with a spatial resolution of up to a few microns per pixel can be obtained through XMT and can be used directly by the LBM—a digital equivalent of the conventional CFD that is more adept at dealing with solid boundaries of complex geometry such as filter media—to calculate flow distribution through the porous structure. An example of this approach using glass beads is described here, from which the permeability of sediments containing this material can be predicted on the basis of a bench-top test and the use of fluid flow simulations. The ability to derive performance information—such as fluid permeability from laboratory-based measurements of microstructure coupled with appropriate microscale physical simulations—has considerable potentials. It is proposed that the method may be used to predict trends such as the filtration behavior of porous structures under different states of compression. This offers a significant benefit in assisting the formulation design of flocculated materials pertinent to a number of industrial sectors wishing to design optimal filtration or relevant operations. © 2006 American Institute of Chemical Engineers *AIChE J,* 52: 3394–3400, 2006
Keywords: microstructure, X-ray microtomography, Lattice–Boltzmann method, permeability, filtration

Introduction

Separation of solids from a suspending liquid is an integral part of many processes. A common practice to recover ultrafine coal, for example, is to flocculate the small particles into larger aggregates before dewatering, thus helping to improve the filtration rate by lowering the cake resistance and also preventing blockage of the filter medium.[1] The microstructure of filter cake has been shown to be responsible for the kinetics of cake formation and desaturation.[2] In general, small and compact aggregates seem to be more suited for filtration than large and loose aggregates, which tend to form compressible cakes and contain more intraparticle moisture.[3]

The process of dewatering involves fluid flowing through

Correspondence concerning this article should be addressed to C. Selomulya at cordelia.selomulya@eng.monash.edu.au.

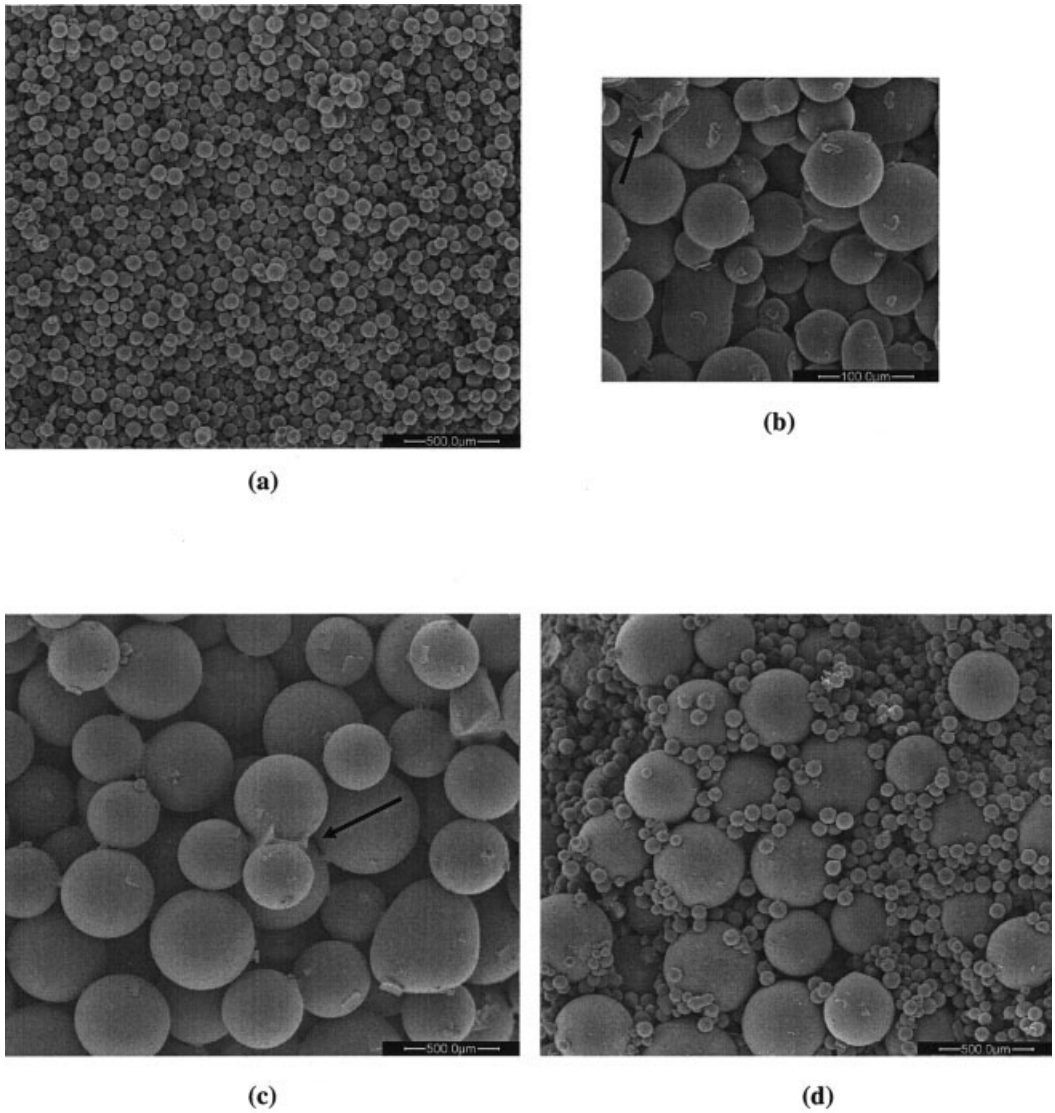

Figure 1. SEM microphotographs showing the cross section of filter cakes composed of (a) 80 μm glass beads (S100) captured at 100× and (b) 500× magnification; (c) 531 μm glass beads (L100) at 100× magnification; and (d) mixture of 80 and 531 μm glass beads (L20–S80) at 100× magnification.

Black arrows indicate some of the larger salt crystals.

porous media. Although most existing data on filtration, sedimentation, and thickening are focused on macroscale phenomena, the challenge is to establish the relationship between solid properties at microscale (pore structure and connectivity) and the overall flow properties of the media.[4] In practice, the characterization of microstructure of porous media can be done by techniques such as imaging, porosimetry, gas adsorption, or capillary filtration, which basically measure the porosity/pore size distribution and/or surface area. Information such as permeability is usually estimated from the structural data by semiempirical functions such as the Kozeny–Carman equation, which uses structure-averaged parameters (porosity, equivalent particle size, and tortuosity) and a validity range limited to granular, close-packed porous medium with solid volume fraction > 0.3. Although other models covering lower solid fractions or nonspherical particles are available,[5] the input parameters still need to be obtained from idealized porous structures.

Recent development on using a digital approach to model packing for objects of arbitrary shapes demonstrated the prospects for predicting the structure and density of sediments by using exact, rather than idealized, representations of complex particulate assemblies.[6] Simulation tools such as the Lattice–Boltzmann method (LBM) to compute and visualize fluid flow and pressure drop across porous media could be applied using these digitized representations. The scope for future use of this concept is based on using imaging techniques to capture real objects in 3-D images and to integrate these data directly with property simulation methods for modeling purposes. Ultimately such an approach offers a more "realistic" simulation because it will effectively enable measurement and property prediction from the same physical sample, while bypassing the need to simplify or stipulate parameters in describing complex shapes.[7] An example of potential applications is in filter design and optimization, of which the process is currently empirically

based, with little fundamental understanding of the significant factors involved, not to mention time-consuming and costly.

Structural imaging of particulate systems in their native state can be conducted using high-resolution X-ray microtomography (XMT) in a relatively nondestructive manner. Examples using glass beads are described here, from which the permeability of sediments containing this material produced from pressure filtration was predicted by tomographic imaging of their microstructures combined with LBM-based simulations. The ultimate aim will be to develop an integrated methodology to derive performance information such as fluid transport properties from microscale measurements and physical simulations, which may be used to predict trends such as the filtration behavior of porous structures under different states of compression. If successful, the method offers a significant benefit in assisting the formulation design of flocculated materials pertinent to a number of industrial sectors wishing to design optimal filtration or relevant operations. The study here highlights the preliminary efforts and challenges faced in developing such procedure.

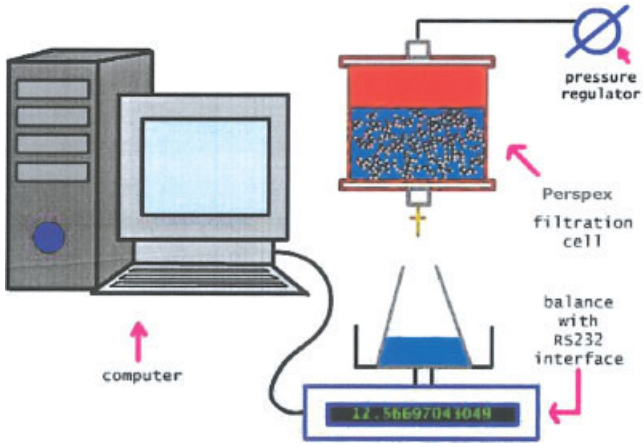

Figure 2. Bench-top hyperbaric filtration system.

[Color figure can be viewed in the online issue, which is available at www.interscience.wiley.com]

Experimental

Materials

Spherical glass beads (Sigma-Aldrich) of <106 μm and 400–600 μm size range were used as model systems. The volume-based mean diameters were measured with a Malvern Mastersizer (Malvern Instruments, Worcestershire, UK) as 80 ± 3 and 531 ± 7 μm, respectively. A mixture of these glass beads (mass ratio of small to large glass beads of 4:1) was also used, giving an averaged volume-based mean diameter of 178 ± 6 μm. The glass beads were washed with 25 wt % HCl solution to dissolve any impurities, followed by repeated washing with Milli-Q water (Millipore Corp., Billerica, MA) before use. A saturated solution of NaCl (Ajax Finechem, Sydney, Australia) was prepared by mixing 150 g of salt in 500 mL of water and filtering out the undissolved solids. The electrolyte was mainly used to bind, rather than to aggregate, the glass beads in filter cakes when dried. The scanning electron microscopic (SEM) images displaying the cross section of filter cakes composed of 80 μm glass beads (S100), 531 μm glass beads (L100), and a mixture of 80 and 531 μm glass beads (L20–S80) at various magnifications are shown in Figure 1. The crystallized salt particles (indicated by the black arrows in Figure 1) were generally small in comparison to the glass beads and thus should not significantly affect the reconstruction of the cake's internal structures.

Filtration tests

The filtration tests were conducted with a 200-mL bench-scale air-pressurized (hyperbaric) filter setup (Figure 2). The purpose of these tests was to indirectly estimate the permeability of preformed cakes composed of spherical glass beads, from the measured filtrate volume with filtration time. A blank run to measure the filter medium resistance was conducted by passing 250 mL of saturated NaCl solution through the 50-mm internal diameter Perspex filter cell fitted with Whatman© filter paper Grade No. 44 with 3 μm size particle retention, at a constant pressure of 10 kPa. The relatively low pressure was selected so that no further structural changes in the preformed filter cake were encountered during the filtration run. The filtrate removed during filtration was collected in a flask placed on a balance, with the weight recorded with time. Glass beads (30 g) were placed into 250 mL of saturated NaCl solution, before being transferred into the filtration vessel. A mechanical stirrer was used to mix the suspension for the first 5 min, before the stirring rate was reduced to allow the glass beads to slowly settle. After the stirrer was turned off, the bed was allowed to form for another 30 min, before filtration started at a constant pressure of 10 kPa.

Specific cake resistance (α) was estimated from the slope of a linear plot between t/V and V, where t is the filtration time and V is the cumulative filtrate volume[8]

$$\frac{t}{V} = \frac{\alpha \mu c}{2A^2 \Delta P} V + \frac{\mu R}{A \Delta P} \tag{1}$$

where μ is fluid viscosity, c is the solid content per unit volume of liquid, A is the filter surface area on which the cake forms, R is resistance of the filter medium, and ΔP is the pressure drop across the filter. For compressible cakes, α varies with ΔP. The cake permeability (k) was derived from

$$k = \frac{\alpha w}{L} \tag{2}$$

where w is the mass of solids deposited per cross-sectional area of the cake and L is the thickness of filter cake. The normalized or specific permeability (k') is reported as k/r^2, where r is the characteristic length scale (that is, average particle radius). Cake porosity (ε) was estimated from the weight of the dry filter cake and its volume, knowing the density of glass beads. For comparison, the specific permeability according to the Kozeny–Carman equation is given as

$$k' = \frac{4\varepsilon^3}{180(1-\varepsilon)^2} \tag{3}$$

Tomographic imaging of microstructures

After the filtration run ended, the filter cake was removed from the cell after 5 min of desaturation time and its thickness recorded. It was then dried inside a desiccator under vacuum overnight (Figure 3a). The thickness measured after drying did not differ from that of the wet cake, indicating that no significant change from the original cake configuration occurred as a result of drying. Samples (about 4 × 4 × 8 mm) were cut carefully, using a sharp Stanly knife from up to six different locations within the cake, and glued onto a piece of wooden skewer that was then fitted into the sample holder (Figures 3b and 3c). With any physical sampling process, this raised the issue of whether the structural integrity of the samples was compromised as a result. In this case, pieces cut from the filter cake were sufficiently strong to maintain their structures (that is, no changes in structure were observed during X-ray tomographic imaging, which took about 25–30 min for the entire scan). Sampling error was also minimized by ensuring that reconstruction of 3-D images was conducted only on the center of each sample, excluding the areas where the cuts were made during sectioning. This procedure should minimize the difference between the original filter cake structure and the resulting microstructure captured by 3-D imaging.

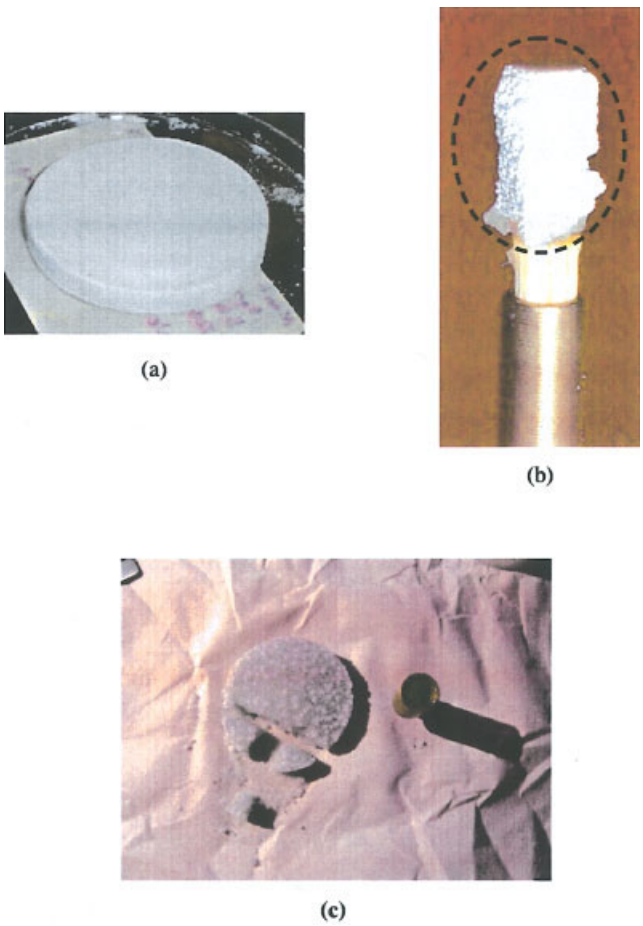

Figure 3. (a) Dry filter cake of 50 mm diameter; (b) a section of filter cake (4 × 4 × 8 mm) composed of 80 μm glass beads attached onto a sample holder; (c) sections of L20–S80 filter cake prepared for scanning.

[Color figure can be viewed in the online issue, which is available at www.interscience.wiley.com]

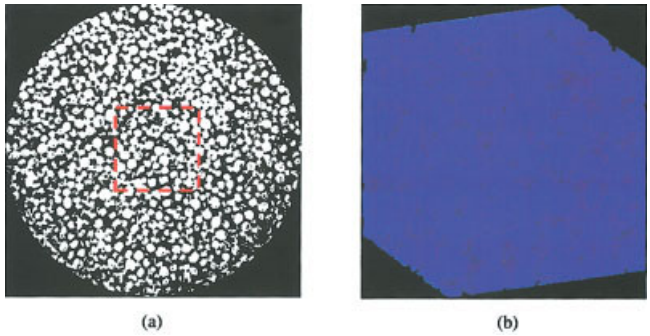

Figure 4. (a) Example of a reconstructed 2-D tomogram (1024 × 1024) showing a horizontal cross section of the filter cake; (b) 3-D volume (250 × 250 × 250) composed of stacked 2-D slices from the region indicated by the dotted line in (a).

[Color figure can be viewed in the online issue, which is available at www.interscience.wiley.com]

An XMT unit, Skyscan-1072, with an 80-keV X-ray source and a 1-mm aluminum filter, was used to scan the sample every 0.45° for 180° rotation at 150× magnification (maximum). The images were then reconstructed from the data set using the cone-beam CT-reconstruction program bundled with the scanner. An image analysis program, ImageJ (http://rsb.info.nih.gov/ij/index.html), was used to "clean" the reconstructed images, by filling the solid regions and removing pixels from the void regions. The 2-D slices were stacked and processed using an in-house code developed at Leeds University before incorporating them onto fluid simulation (Figure 4).

Fluid simulation

The 3-D images were subsequently used with the LBM to model flow distributions through the porous media. The basic feature of LBM is to track discrete fluid "particles" of variable densities with discrete velocities in a lattice grid that maps the space.[9] Although rooted in kinetic theory for gas, formulated and performed in a lattice setup, LBM can be shown to recover the Navier–Stokes equations under low Mach number conditions. A major advantage of using such a lattice-based model is that solid boundaries can be directly incorporated, given that XMT-imaged microstructures are also digitally specified in a lattice grid. This circumvents the complexities of a separate mesh generation required by traditional computational fluid dynamics (CFD) programs. An example of a commercial package based on an extension of the Lattice Gas/Boltzmann Model is PowerFLOW® from EXA Corp. (Burlington, MA). The software allows solid geometry, whether computer generated or directly imaged, to be imported as a closed surface defined by triangular facets, after which each surface voxel is generated independently of its neighbors. The disadvantage of this approach is that it requires enormous computational power to resolve larger volume and/or complex structure. In this work, the program was run on dual AMD Opteron 244 processors with 8GB RAM.

Another code developed at the University of Leeds, DigiFlow®, was also used in this work for comparison. The kernel

Table 1. Properties of Filter Cakes Composed of Glass Beads as Determined from Filtration Tests

Property	Sample		
	S100	L100	L20–S80
Glass beads	80 μm	531 μm	Mixture of 80 and 531 μm (mass ratio 4:1)
ΔP (kPa)	10	10	10
L (m)	$(1.06 \pm 0.02) \times 10^{-2}$	$(1.08 \pm 0.02) \times 10^{-2}$	$(1.08 \pm 0.04) \times 10^{-2}$
ε	0.39 ± 0.02	0.37 ± 0.03	0.41 ± 0.02
k'	$(2.97 \pm 0.38) \times 10^{-3}$	$(1.72 \pm 0.47) \times 10^{-4}$	$(1.07 \pm 0.12) \times 10^{-3}$
k' (Kozeny–Carman)	$(3.68 \pm 0.68) \times 10^{-3}$	$(4.74 \pm 1.18) \times 10^{-3}$	$(2.93 \pm 0.79) \times 10^{-3}$

is based on Hoffman's implementation of the so-called D3Q19 LBM scheme.[10] The program is built with a graphical user interface for input/output, a volume rendering routine for visualization, and is multithread enabled for shared memory parallel computing platforms such as the dual CPU PC workstation mentioned above. Therefore, in contrast to the general-purpose PowerFLOW®, DigiFlow® is specifically designed to facilitate the calculation of permeability of digitally specified porous media from either XMT imaging or a computer model such as DigiPac®. After a number of iteration or evolution steps, the flow reaches a steady state so that a normalized intrinsic permeability can be estimated directly from the calculated superficial velocity and some input model parameters as

$$k' = \frac{U(2\tau - 1)}{6 f_b a^2} \tag{4}$$

where U is the calculated superficial velocity, f_b is a body-force driving the fluid flow (equivalent to pressure gradient), τ is a relaxation parameter related to the kinematic viscosity (in lattice units) by $\nu = \eta/\rho = (2\tau - 1)/6$, and a represents the mean radius of particles used for scaling. All parameters are in lattice units, with f_b and τ as input parameters set to 0.001 and 1, respectively, for all simulations. Other things being equal, as the microstructure changes, so does the calculated flow velocity and thus the permeability. It is therefore crucial to obtain as accurate representations of the microstructure as possible for fluid flow simulation through these porous media. In addition to the superficial velocity, LBM provides details of flow distribution inside every channel of the pore network in the porous medium, from which flow uniformity or channeling can easily be identified and visualized, and the relationship between microstructure and flow distribution be assessed.

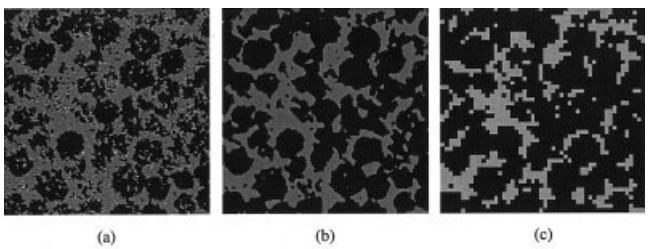

Figure 5. (a) A 250 × 250 section before "cleaning" and (b) after cleaning as used in DigiFlow®; (c) a scaled-down version as used in PowerFLOW®.

Dark sections indicate where the solids are.

Results and Discussion

Cake properties

A summary of the filter cake properties composed of different size glass beads is shown in Table 1. The data were obtained based on filtration tests conducted in triplicate. The indirect measurement of permeability from specific cake resistance was subject to uncertainties arising from the small sample size, as well as errors in determining the mass of solids per cross-sectional area and cake height, and the slope of plot between t/V and V. On the other hand, fluid transport depends mainly on the connectivity of the pores, rather than properties such as porosity or solid volume fraction,[11] so that theoretical formulations based on these parameters (such as k' estimated from the Kozeny–Carman equation) could yield inaccurate estimations. A recent study[12] also demonstrated that the majority of flow is carried by "active" pores (or flow channels), which is in relatively small proportion compared to the total pore volume (that includes dead pores). In this case, the cakes formed by 80 μm glass beads (S100) showed the highest specific permeability, followed by those formed by a mixture of glass beads of different sizes (L20–S80) and 531 μm glass beads (L100), despite the filter cakes estimated as having relatively comparable porosity values from the measurement of cake thickness and mass.

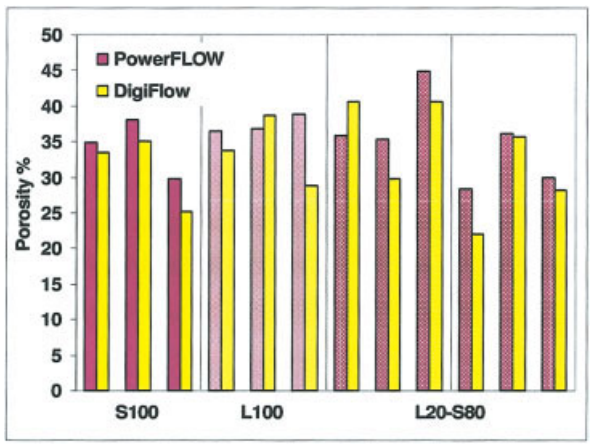

Figure 6. Local porosity values as estimated from 3-D images of microstructures for PowerFLOW® and DigiFlow®.

[Color figure can be viewed in the online issue, which is available at www.interscience.wiley.com]

Table 2. Comparison of Averaged Porosities as Determined from Experiments and from 3-D Images of Microstructures

Property	Sample		
	S100	L100	L20–S80
Measured ε	0.39 ± 0.02	0.37 ± 0.03	0.41 ± 0.02
Estimated ε for PowerFLOW®	0.34 ± 0.04	0.37 ± 0.01	0.35 ± 0.06
Estimated ε for DigiFlow®	0.31 ± 0.06	0.34 ± 0.05	0.33 ± 0.07

Permeability estimation through reconstructed microstructures

In this study, prediction of permeability was done by simulating fluid flowing through the porous microscale structures. Because permeability is an intrinsic structural property by definition, it can be estimated according to Darcy's law by applying a certain pressure gradient across the structure and measuring the flow velocity. Two LBM codes, PowerFLOW® and DigiFlow®, respectively, were used to model fluid distribution through the microstructures.

Up to six samples taken from different locations across the filter cakes were scanned with X-ray microtomography and their 3D configurations obtained from the reconstructed tomograms at 1.77 μm/voxel. In PowerFLOW®, the structure needs to be imported as a closed surface (such as STL, ANSYS) before their surface voxels ("surfels") were regenerated individually. This facetization of geometry puts a considerable demand in memory and thus the choice of resolution is usually a trade-off between the accuracy and resources available. For example, to re-create a structure contained in a 10-MB STL file, the simulation grid containing information of individual fluid voxels and solid surfels, as well as the initial conditions and dynamic parameters, could easily reach >1 GB. On the other hand, DigiFlow® works directly with the stacked volume in a binary format without further processing and thus can handle larger scales than PowerFLOW® with the same computing resources.

Two hundred fifty slices (250 × 250 lattice units) taken from the center region of the tomograms (1024 × 1024) were "cleaned" and stacked into a binary format for use with DigiFlow®. In PowerFLOW®, the same region was scaled down to 20% before conversion to STL to reduce the memory requirement, giving a sample size of 50 × 50 × 50 (Figure 5). The reconstructed images were then analyzed using CT-analyzer, with volume fraction estimated from the number of solid voxels enclosed in that volume, indicating the local properties at that particular section of the cake. Sources of errors at this stage were mainly introduced by thresholding of the reconstructed cross sections and image filtering. The tomograms were in the form of bitmap images in a gray scale (Figure 4a). The 3-D model of the structure was built by assuming the white pixels as solid and the black pixels as void, so that the choice of threshold limit was crucial. Image filtering was also done to remove or add stray pixels from/to solid/void areas. In this case, if there were fewer than 20 black pixels in regions identified as solids, they would be removed, whereas fewer than 10 white pixels in regions identified as voids would be filled by black pixels.

Porosity estimated from images used in PowerFLOW® and DigiFlow® are shown in Figure 6. In general, the values were higher for PowerFLOW®, possibly as a result of the coarser

Table 3. Boundary Conditions for Simulations by PowerFLOW® and DigiFlow®

PowerFLOW®	DigiFlow®
3-D laminar, isothermal flow	3-D laminar, isothermal flow
ΔP: 50 Pa	All dimensional parameters in lattice units
Fluid density: 1000 kg/m^3	f: 0.001 (body force or pressure gradient)
Fluid kinematic viscosity: 10^{-6} m^2/s	τ: 1 (relaxation parameter)
Scaling radii: 40 μm (S100)	ν: 1/6 (kinematic viscosity)
266 μm (L100)	Scaling radii: 20 (S100)
89 μm (L20–S80)	50 (L100)
Total time steps: 5000	22 (L20–S80)
Equivalent of one time step: 1.7×10^{-6} s	Total time steps: 3000
Simulation volume size: 50 × 50 × 50	Simulation volume size: 250 × 250 × 250

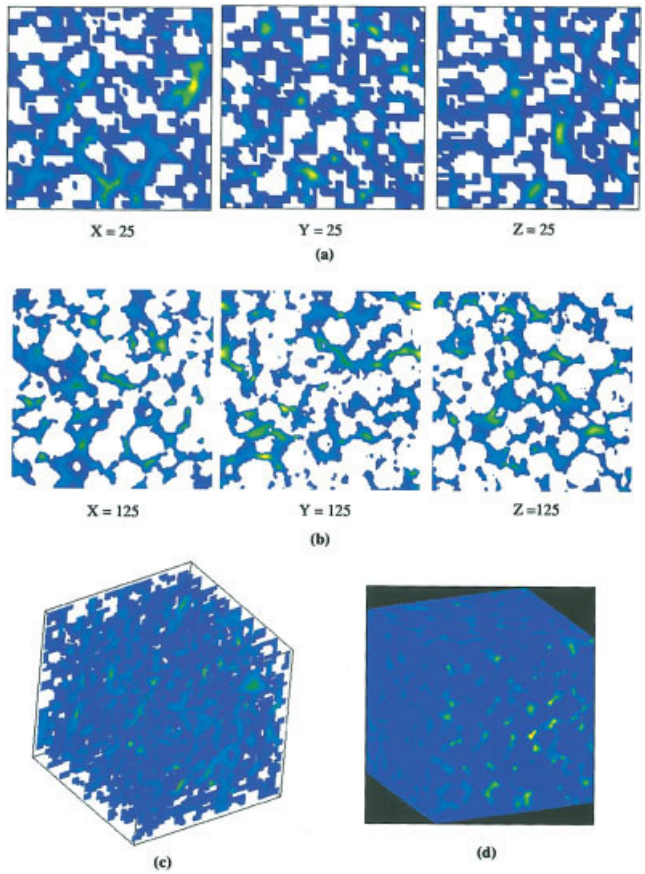

Figure 7. Examples of velocity distribution on an S100 structure on slices taken at X, Y (where superficial velocity is calculated), and Z coordinates denoting the midsection of the structure from (a) PowerFLOW® and (b) DigiFlow®; lower resolution in PowerFLOW® clearly influenced its overall velocity distribution (c) in comparison to the velocity distribution obtained from DigiFlow® (d).

[Color figure can be viewed in the online issue, which is available at www.interscience.wiley.com]

Table 4. Comparison of Specific Permeability k' Determined from Experiments and from Fluid Flow Simulations Using 3-D Images of Microstructures

Property	Sample		
	S100	L100	L20–S80
k' from filtration tests	$(2.97 \pm 0.38) \times 10^{-3}$	$(0.17 \pm 0.04) \times 10^{-3}$	$(1.07 \pm 0.12) \times 10^{-3}$
k' from PowerFLOW®	$(1.51 \pm 0.56) \times 10^{-3}$	$(0.57 \pm 0.08) \times 10^{-3}$	$(0.74 \pm 0.51) \times 10^{-3}$
k' from DigiFlow®	$(0.57 \pm 0.08) \times 10^{-3}$	$(0.50 \pm 0.29) \times 10^{-3}$	$(0.85 \pm 0.26) \times 10^{-3}$

resolution used. Although local porosity determined in this manner was not free from errors associated with sample handling, reconstruction, and digitization, the estimated averaged porosity from the microstructures was found to be comparable to the overall porosity determined experimentally (Table 2).

The boundary conditions for simulations by PowerFLOW® and DigiFlow® are listed in Table 3. The parameters were given in SI units for PowerFLOW®, whereas DigiFlow® used lattice units. The difference in units would not affect the estimation of specific permeability k', reported as normalized by the characteristic length scale. The characteristic length scale was the averaged particle radius (in μm) for PowerFLOW®. In DigiFlow®, the equivalent scaling radius in lattice units was measured for a typical sphere from the cross-sectional images of the visible structures actually used for simulations. In PowerFLOW® simulation, the pressure gradient (ΔP) was set to 50 Pa in the Y-direction of flow, and the simulation was conducted until there was no further change in the Y-velocity over a number of time steps (the pressure gradient value was chosen to provide relatively fast convergence with acceptable stability in this case—the choice should not affect permeability estimation, which is an intrinsic structural property). Figure 7 shows examples of the distribution in velocity values for an S100 structure. The slices were taken at X, Y, and Z coordinates of the midsection from the images used in PowerFLOW® (with coarser resolution) and DigiFlow®, respectively. The superficial velocity (U) was calculated from the sum of Y-velocity divided by the cross-sectional area of the center slice normal to the direction of the flow, and the permeability estimated based on Darcy's equation

$$k = \frac{U\mu l}{\Delta P} \tag{5}$$

where l is the length of the structure. Area-based superficial velocity was also used to calculate k' in DigiFlow® according to Eq. 3.

The predicted k', averaged from values obtained in fluid simulations on several samples of the filter cakes, is listed in Table 4. The values were within a similar order of magnitude with those determined from filtration tests. This implied that the microscale structures in this case were reasonably indicative of the bulk solid. The relatively large standard deviation on k' was partly attributable to the structural variation between the images used in fluid simulations and thus highlighted the need to use a sufficient amount of data (or images in this case) to achieve a better statistical representation of the overall properties, which currently is still limited by computational resources and imaging capability. Nonetheless, the methodology presented here shows the potential for quicker and more accurate assessments, especially for small samples for which measurements are particularly difficult to obtain because of wall effects, that is, by conducting the entire tests virtually on a computer.

Conclusions

A procedure for sampling, imaging, and integrating structural information, obtained from filter cakes containing spherical glass beads, with fluid simulation tools was outlined here. The results indicated that the methodology proposed here is sufficiently robust to be used for predicting overall system characteristics based on microscale measurements. Current limitations arise from demands placed on computational resources to simulate a large amount of data for adequate representation of the bulk properties, in addition to the existing imaging capability. Nevertheless, the study introduced a proof of concept for such analyses to be performed, potentially on a routine basis in the future.

Literature Cited

1. Tao D, Parekh BK, Liu JT, Chen S. An investigation on dewatering kinetics of ultrafine coal. *Int J Miner Process.* 2003;70:235-249.
2. Bourgeois FS, Barton WA. Advances in the fundamentals of fine coal filtration. *Coal Prep.* 1998;19:9-31.
3. Gregory J. The role of floc density in solid–liquid separation. *Filtr Sep.* 1998;35:367-371.
4. Lin CL, Miller JD. Pore structure analysis of particle beds for fluid transport simulation during filtration. *Int J Miner Process.* 2004;73:281-294.
5. Kim AS, Stolzenbach KD. The permeability of synthetic fractal aggregates with realistic three-dimensional structure. *J Colloid Interface Sci.* 2002;253:315-328.
6. Jia X, Williams RA. A packing algorithm for particles of arbitrary shapes. *Powder Technol.* 2001;120:175-186.
7. Williams RA, Jia X. Tomographic imaging of particulate systems. *Adv Powder Technol.* 2003;14:1-16.
8. Orr C. *Filtration: Principles and Practice*. New York: Marcel Dekker; 1977.
9. Succi S. *The Lattice Boltzmann Equation: For Fluid Dynamics and Beyond* (Numerical Mathematics and Scientific Computation Series). Gloucestershire, UK: Clarendon Press; 2001.
10. Hoffman HW. A 3D lattice Boltzmann code for modelling flow and multi-component dispersion. Sandia Report SAND99-0162. Livermore, CA: Sandia National Laboratories; 1999.
11. Martys NS, Torquato S, Bentz DP. Universal scaling of fluid permeability for sphere packing. *Phys Rev E.* 1994;50:308-403.
12. Xu C, Jia X, Williams RA. Use of Lattice Boltzmann method to facilitate characterisation of pore networks in porous media. Proceedings of the 2nd Particulate Systems Analysis, Stratford-upon-Avon, UK, Sep. 21–23; 2005.

Manuscript received May 12, 2006, and revision received Jun. 22, 2006.